Topics in Catalysis (2024) 67:615–627
https://doi.org/10.1007/s11244-024-01916-w

ORIGINAL PAPER

Synthesis and Characterization of NiMoS/TiMg and NiWS/TiMg Nanocatalysts and Their Application in the Hydrodesulfurization of Dibenzothiophene

P. Peña-Obeso[1] · M. E. Cervantes-Gaxiola[2] · J. L. Rico[1] · J. N. Díaz de León[3] · S. Guevara-Martinez[1] · J. A. Lumbreras-Pacheco[1] · R. Huirache-Acuña[1]

Accepted: 29 January 2024 / Published online: 12 March 2024

Abstract

NiMoS/TiMg and NiWS/TiMg nanocatalysts were synthesized, characterized by various techniques and tested in the hydrodesulphurization (HDS) of dibenzothiophene (DBT). TiMg mixed oxides containing 5, 10 or 15 wt% of MgO were prepared by sol–gel and then used as catalyst supports. A constant atomic ratio of Ni/(Ni + M) = 0.5 was kept for all the catalysts (M = Mo or W). The catalysts were first prepared by sequential-wet impregnation. Then, after an ex-situ sulfidation process, they were characterized by high resolution transmission electron microscopy (HR-TEM), X-ray diffraction (XRD), and physisorption of N_2 following the BET method. The presence of MgO in the NiMoS/TiMg and NiWS/TiMg catalysts resulted in an enhancement in the HDS activity of DBT. In addition, their HDS activities were higher than those observed in the NiMoS/Ti and NiWS/Ti catalysts. Furthermore, higher HDS activity was found for the NiMoS/TiMg compared with their NiWS/TiMg catalysts counterpart.

Graphical Abstract

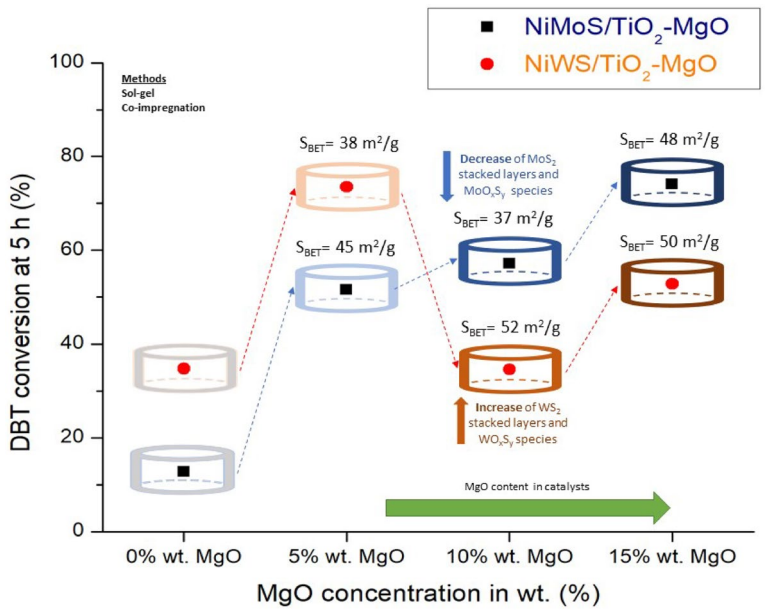

Keywords Hydrodesulfurization · Dibenzothiophene · TiMg mixed oxides

Extended author information available on the last page of the article

1 Introduction

The new worldwide environmental regulations are demanding fuels with low pollutant content to reduce the contamination of the atmosphere [1]. The presence of sulfur and nitrogen organic compounds is one of the most important challenges facing refineries to get cleaner fuels, since these chemical contaminants are present in crude oil [2]. Moreover and according to the World Energy Review [3] most of the crude oil reserves still available have high pollutant contents, especially sulfur and nitrogen organic compounds. Molybdenum and tungsten sulfides promoted with Ni or Co and supported on alumina are among the most common catalysts used in hydrotreating (HDT) [4–7]. However, these catalysts do not fulfil the new environmental regulations related to ultra clean fuels. One of the alternatives to address this problem is to develop new and more effective catalysts to comply with the environmental regulations. To this aim, alternatives such as a catalyst synthesis method, nature of the active phase and catalyst support are proposed [8]. The effect of the support on the catalyst behavior is a very important subject, since the metal-support interactions influence the dispersion, morphology and activation of metals [9]. Several research works related to the modification of alumina or titanium supports in hydrotreating catalysts such as TiO_2–Al_2O_3 [10], Al_2O_3–TiO_2–MgO [11], Al_2O_3–MgO [12–15], Mg–TiO_2 [16] have been reported. Lopez Agudo et al. [10] studied the effect of titanium into alumina by preparing Mo, CoMo and NiMo supported samples. The addition of a small amount of Ti ($x \leq 0.8$ and x defined as a molar ratio equal to $TiO_2/(Al_2O_3 + TiO_2)$) into alumina, some Co was dispersed into the alumina matrix resulting in a decrease in the HDS activity. Higher Ti loadings improve the HDS of thiophene. In another publication, Espino-Valencia et al. [11] studied the effect of MgO into the support. In this study Al–Ti mixed oxides (Al/Ti atomic ratio of 5.7) modified with MgO (0, 5, 10, 15 wt%) were synthetized by sol–gel and used as supports to prepare NiMoW sulfide catalysts. All catalysts presented an atomic ratio of Ni/(Ni + Mo + W) equal to 0.5 and the best catalyst in the HDS of DBT was observed for the NiMoW/Al–Ti–Mg sample containing 5 wt% of MgO. The beneficial effect of MgO was probably related to an increased dispersion of the active species, when the physicochemical properties of the support were improved. Ancheyta et al. [12] prepared CoMo catalysts supported on MgO-alumina of 0.01, 0.1 and 0.5 $MgO/(MgO + Al_2O_3)$ ratios. Their results showed that when increasing the MgO content, the stability of the catalyst and the activity in the HDS of thiophene were enhanced. Ramirez et al. [13], synthetized Mo and NiMo catalysts supported on Mg–Al mixed oxides with x = $MgO/(MgO + Al_2O_3)$ molar ratios equal to 0.0, 0.05, 0.25, 0.50, 0.75 and 1.0 by sol–gel and tested in the HDS of thiophene. The results indicate that the hydrogenation is substantially reduced if small amounts of magnesia are incorporated, changing also the HDS activities. These effects were probably due to the formation of $MgMoO_4$ and NiO–MgO. The results also indicate that only the catalysts with low magnesia content ($x < 0.25$) show textural stability. In another research work, Guevara-Lara et al. [14] synthetized two Mg–Al mixed oxides containing 95 and 80 mol% of MgO by sol–gel, and then used as supports to prepare Ni and NiMo catalysts. The dried (D) and calcined (C) samples were sulfided and then tested in the HDS of DBT. The promotional effect of Ni on the HDS of DBT was only observed for the catalyst with 95 mol% of MgO. The characterization indicated that during impregnation, the interaction of MoO_4^{2-} and the support was strong and increased after calcination. The authors reported a Ni promoting effect, defined as (NiMo catalyst rate)/(Mo catalyst rate), of 4.5 and 8.5 for the dried and calcined NiMoMg95Al5 sulfided catalysts, respectively. Among the prepared samples, the best HDS catalytic activity was observed with the NiMoSMg95Al5-C sample. In another publication, Guevara-Lara et al. [15] reported the effect of magnesium by testing the NiW/Al_2O_3 and NiW/Al_2O_3-MgO catalysts on the HDS of DBT. For this purpose, the alumina support was modified with 5 mol% of MgO during the sol–gel synthesis. After preparation of the supports, co-impregnation with Ni and W at pH of 4 or 9 was performed. The authors found during the catalytic tests that the catalysts prepared at pH 9 showed lower HDS activities than those prepared at pH of 4, probably due to a stronger Ni–W interactions present in the former catalysts. In addition, the NiW/Al_2O_3–MgO samples prepared at pH of 4 showed better catalytic activities than that measured for the commercial $NiWS/Al_2O_3$ sample. The authors found a favorable outcome when adding MgO into alumina during the HDS of DBT. Díaz de León et al. [16] reported the synthesis of NiW supported on MgTi mixed oxide (containing 10, 25, 50 mol% of TiO_2). The effect of drying and calcination were also taken into account. All catalysts contain 26 wt% of WO_3 and 4 wt% of NiO. The dried NiWS sample, co-impregnated in aqueous medium and supported on a MgTi oxide with 25 mol% of TiO_2 showed the highest catalytic activity in the HDS of DBT among the MgTi supported samples.

The aim of present research project was the modification of titanium oxide with low quantities of Mg and to use these oxides as supports to prepare NiMo/TiMg and NiW/TiMg sulfide nanocatalysts. For comparison, similar catalysts without magnesium were also synthetized and used as reference. Finally, the effect of magnesium on the HDS of DBT was evaluated. To our knowledge the effect of small

quantities of magnesium in these catalysts for this reaction has not been previously reported.

The objective of this research project was to modify titanium oxides with low quantities of MgO and compare them to those reported in the literature. Then, mixed oxides as supports were used to prepare NiMo/TiMg and NiW/TiMg sulfide nanocatalysts. The final effect was evaluated in the HDS of DBT.

2 Experimental

2.1 Synthesis of Supports

The TiMg mixed oxides with 0, 5, 10 and 15 wt% of MgO were synthesized by sol–gel. For this purpose, the required titanium butoxide was added into 150 ml of isopropanol and mixed during 1 h at 60 °C. The solution was then cooled down to 3 °C. An aqueous solution containing water, ethanol, isopropanol, nitric acid in a ratio 13:8.5:5:0.5 v/v, with the required amount of magnesium, using $Mg(NO_3)_2{\cdot}6H_2O$ as a precursor, was prepared. Once the temperature of 3 °C was reached, the aqueous solution was added dropwise very slowly to the isopropanol mixture till the formation of a gel. The gel was aged in a fridge during 24 h and then dried in air and calcined in an oven. To calcine the samples, they were heated at 10 °C/min, from ambient temperature to 500 °C. Then the remaining substance was allowed to stand for 4 h at the final temperature reached. The obtained powder was then pressed to make pellets and then pulverized to finally select particle sizes of 25–40 mm using sieves. The solids were labelled as TiMg 5, TiMg 10 and TiMg 15 according to the weight percent of MgO used during synthesis.

2.2 Synthesis of Catalysts

A constant Ni/(Ni + M) atomic ratio equal to 0.5 was used in all catalysts. In the expression M = Mo or W. Besides, Ni and Mo (or W) contents of 18 wt% were also utilized in all samples. The required quantities of ammonium heptamolybdate, $[(NH_4)_6Mo_7O_{24}]$, ammonia metatungstate $[(NH_4)_6H_2W_{12}O_{40}{\cdot}xH_2O]$ and nickel nitrate $[Ni(NO_3)_2{\cdot}6H_2O]$ were separately dissolved in deionized water. Drop-wise sequential impregnation of the supports was then performed. The molybdenum or tungsten solution was first impregnated followed by the nickel solution. After the pores were filled with the solution, the powder was dried at 120 °C for 2 h and the impregnation continued until the whole metal solution was incorporated. Afterwards, the powder was calcined in an oven from ambient temperature to 450 °C, heating at 10 °C/min. A dwell time of 4 h was given. Finally, the samples were ex-situ sulfided under a flow of H_2S/H_2 (15% v/v) at 400 °C during 4 h and finally kept in an inert atmosphere. The catalysts were labelled as NiMoS/TiMg-5, NiMoS/TiMg-10 and NiMoS/TiMg-15

2.3 Characterization of Catalysts

2.3.1 X-ray Diffraction

The diffraction patterns were acquired using a Siemens D-500 equipment provided with a graphite monochromator and using Cu-α radiation with λ = 1.54 Å, at 30 kV and 20 mA, from 5 to 90° 2θ.

2.3.2 Nitrogen Physisorption

The specific surface areas, mean pore size and pore size distribution were determined using nitrogen adsorption-desorption isotherms and the BET method. For this purpose, a Quantachrome equipment was used. All samples were first degassed at 270 °C under vacuum during 5 h. For the determination of the mean pore size and pore size distribution, the BJH was utilized.

2.3.3 High Resolution Transmission Electron Microscopy

HR-Transmission electron microscopy (HRTEM) clear field images were obtained using a JEOL JEM-2200FS (200 kV) (0.23–0.1 nm resolution) microscope in order to get information about $Mo(W)S_2$ slab length and stacking degree. Several zones on the micrographs were observed to perform a statistical analysis of MoS_2 slabs. Samples were ultrasonically dispersed in ethanol before being deposited onto a carbon-coated Cu grid (lacy carbon, 200 mesh).

2.4 Catalytic Activity

The activities for all catalysts were evaluated in the HDS of DBT. The experiments were performed using a high pressure Parr 4560 reactor. In a typical experiment, the reactor was loaded with 0.5 g of the sulfide catalyst and 75 mL of a solution (5% of DBT in *n*-heptane by volume). The reactor was first purged with nitrogen, heated up to 350 °C and then pressured with H_2 at 3.1 MPa, at this moment is taken the first sample. The reactants were continuously stirred. The reaction was carried out during 5 h, taking reaction samples to analyze them using a Hewlett Packard GC (model 4890) chromatograph, which was provided with a HP-Ultra 2 (30 m × 0.32 mm D.I.) column and a FID detector. The kinetic constants (k) were calculated assuming pseudo first order kinetics referred to initial DBT concentration.

$$k \cdot t = \ln\,(1 - x) \tag{1}$$

where t is the reaction time, and x is the conversion of DBT.

The main reaction products in the HDS of DBT were biphenyl (BF), principally produced following the direct desulfurization pathway (DDS), cyclohexylbenzene (CHB) and tetrahydrodibenzothiophene (THDBT) mainly produced following the hydrogenation pathway (HYD). The selectivity between these two pathways was then evaluated:

$$S_{HYD/DDS} = \frac{[THDBT] + [CHB]}{[BF]} \quad (2)$$

2.5 X-ray Photoelectron Spectroscopy

The XPS spectra of the samples were recorded using a SPECS® spectrometer provided with a PHOIBOS® 150 WAL hemispherical energy analyzer with angular resolution (< 0.5°), and equipped with XR 50 X-Ray Al-X-ray and μ-FOCUS 500 X-ray monochromator (Al excitation line) sources. The samples were kept in an argon atmosphere prior to their analysis and transferred into a mobile XPS chamber for degasification. The binding energy (BE) of C 1*s* (284.8 eV) was used as a reference. The BE and intensities for the chemical quantification were determined after subtraction of a Shirley-type background from the photoemission spectra using the Casa XPS software (ver. 2.3.19). The surface elemental composition was evaluated from the experimental areas, corrected by the Scofield photoionization sensitivity factors.

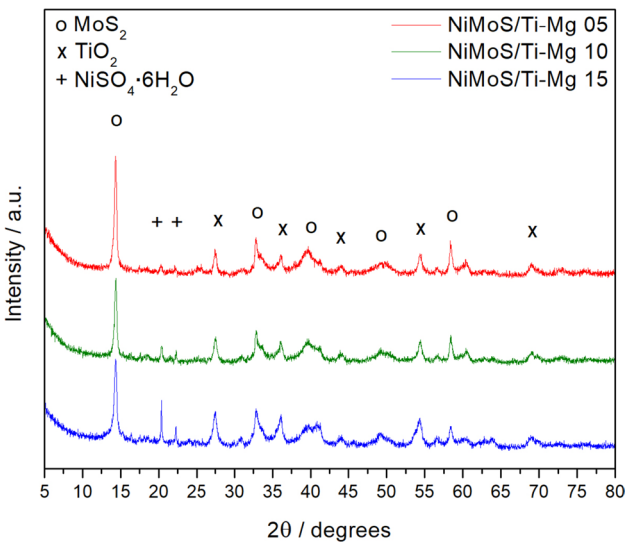

Fig. 1 XRD patterns for NiMoS/TiMg catalysts

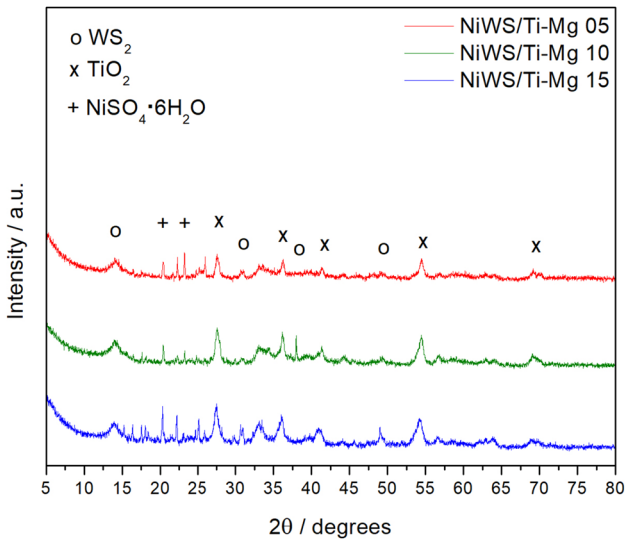

Fig. 2 XRD patterns for NiWS/TiMg catalysts

3 Results and Discussion

3.1 X-ray Diffraction

Figures 1, 2 show the X-ray diffraction patterns of the NiMoS/TiMg and NiWS/TiMg catalysts. The weak diffractions indicate that the structures are poorly crystalline. In both figures, the diffraction at 14, 32, 39, 49 y 58° 2θ are assigned to MoS_2 or WS_2 sulphides [PDF 37-1490, PDF 08-237]. The weak diffraction signals at about 27, 36, 40, 44, 54 and 69° 2θ correspond to the titania-rutile phase [PDF 21-1276]. No diffraction peaks assigned to MgO and/or $Mg(OH)_2$ were observed indicating that Mg species might be amorphously present and/or Mg atoms are well distributed in the solid structure [11]. For the NiMoS/TiMg samples, well-defined narrow diffraction signals at about 14 ° 2θ are noticed, indicating stacking of the metal-sulphide fringes in the "c" direction of the (002) crystalline plane of the hexagonal structure of the MoS_2 [11] whose intensity decreases as the Mg content rises. On the other hand, an increase in Mg makes the diffraction signal greater related to $NiSO_4$ which resulted from the transformation of nickel sulphide to sulphate after exposing the material to air [17]. Comparing the NiMoS/TiMg and NiWS/TiMg catalysts, diffraction signals corresponding to $NiSO_4$•$6H_2O$ were observed in the former series of catalysts. Additionally, the NiWS/TiMg samples are less crystalline than the other series. NiWS catalysts supported on magnesium-modified titanium oxides and their activities were previously reported [16]. However, in that work, the authors have modified MgO with titanium (10, 25 and 50 mol% of TiO_2 in MgO) and detected Mg segregation as $Mg(OH)_2$ in the X-ray diffraction patterns. On the contrary, in the present research work, TiO_2 was modified

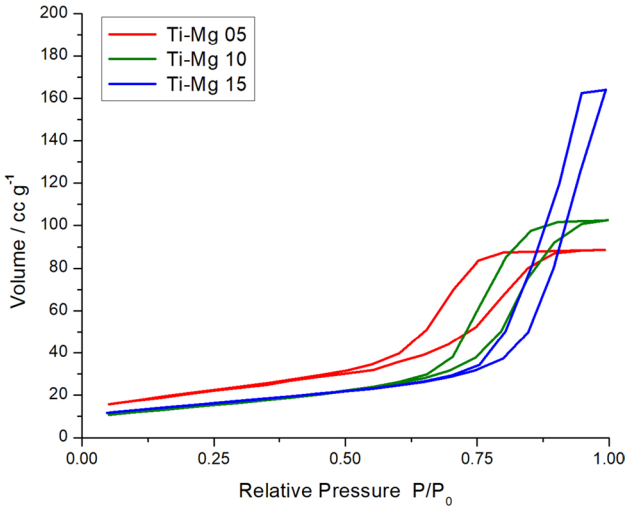

Fig. 3 Nitrogen adsorption–desorption isotherms for the TiMg mixed oxides

Table 1 Textural properties for the TiMg mixed oxides

Mixed oxide	Specific surface area (m^2/g)	Mean pore volume (cm^3/g)	Mean pore diameter (nm)
TiMg 05	86	0.14	6.7
TiMg 10	75	0.17	7.9
TiMg 15	63	0.26	12.6

Specific surface area, mean pore volume and mean pore diameter

with magnesium (9.4, 18 and 25.9 mol% of MgO in TiO_2). Furthermore, Mg is likely well-distributed into the titanium matrix and non-segregation was observed, which could be explained considering the low Mg loadings in our samples compared to those reported by Díaz de León et al. [16].

3.2 Nitrogen Physisorption

Figure 3 shows the adsorption–desorption isotherms of the supports. It can be noticed that the solids exhibit type IV isotherms and H2 hysteresis, indicating that the solids are mesoporous materials with bottleneck pores [18]. In addition, it is observed that an increase in N_2 adsorption as the Mg content in the solids goes up. The determined surface areas were 86, 75, and 63 m^2/g for TiMg-5, TiMg–10 TiMg–15, respectively, showing a decrease as the Mg content increases. Table 1 presents a summary of the textural properties of the supports. It can be noticed that the specific surface areas decrease, whereas the pore volume and the diameter of pores increase as the Mg contents augments. Klimova et al. [13] stated that one of the disadvantages of MgO supported catalysts is that when in contact with moisture, the high surface area MgO is transformed to low surface. In this work, it was observed a decrease in surface area when an increase of MgO content (15%) was used, this behaviour could be related with the formation of low surface $Mg(OH)_2$ since It appears that even upon standing at ambient conditions MgO is converted to a mixture of $MgCO_3$ and $Mg(OH)_2$.

Figure 4 presents the corresponding adsorption-desorption isotherms for NiMoS/TiMg and NiWS/TiMg catalysts. In addition, the volume of N_2 adsorbed increases with increasing Mg content in both series of catalysts. A

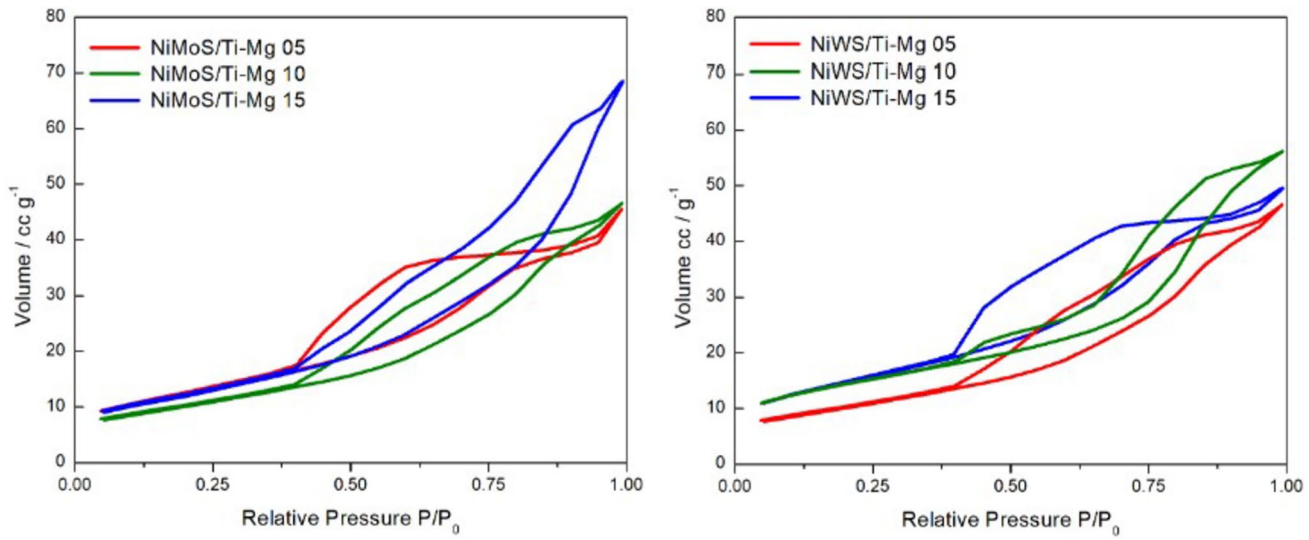

Fig. 4 Nitrogen adsorption–desorption isotherms for the NiMoS/TiMg and NiWS/TiMg samples

slightly change in the hysteresis loop was observed after the incorporation of metals. In the case of the first system, it can be observed that for 05 and 10 loops, the maximum adsorbed value was comparable, however for 15 sample, the value increased by 50% compared with their counterparts. For the system with tungsten. It was observed that the highest adsorption was for Mg10 since a higher amount of N_2 was detected. The amount was approximately 20% higher than that observed for their counterparts. In addition, a pore filling speed at a lower concentration was observed for the NiMoS system in comparison with their NiWS counterparts. The pore size distribution of the supports and the two series of catalysts is presented in Figures 5 and 6. In Fig. 5, a unimodal behaviour can be observed. On the other hand, a difference can be observed depending on the concentration (Fig. 6), showing a unimodal behaviour for samples at lower concentration. While, a bi or multimodal behaviour can be observed for samples at higher concentration. However, it could be observed that all samples show a peak around 4 nm in all cases. As expected, the impregnation of metals on the support decreases the porosity and the specific surface areas. The pore sizes for the NiMoS/TiMg are smaller than those on the NiWS/TiMg samples. The bimodal pore distribution can be related with the incorporation of metals on the support. When the impregnation was used to introduce active phase precursors, metal oxides were distributed from inside out decreasing pore diameter causing the presence of a second peak. Table 2 shows the textural properties of both series of catalysts. Most of the samples present a mean pore size of about 3.4 nm.

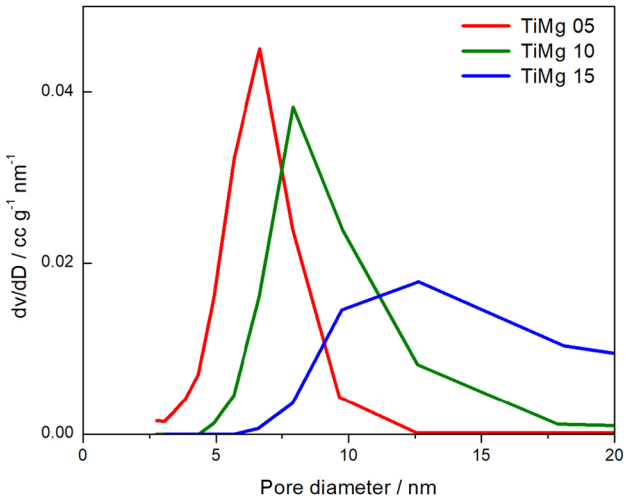

Fig. 5 Pore size distribution of the TiMg mixed oxides

3.3 High Resolution Transmission Electron Microscopy

Micrographs of the NiMoS/TiMg samples containing 5 and 15 wt% of MgO were acquired by HR-Transmission Electron Microscope (HRTEM) and some are presented in Figs. 7 and 8. Stacked fringes characteristic of the (002) basal plane of the metal sulfides are clearly observed [15]. An interplanar distance of 6.3 Å was measured and corresponds to MoS_2 [13]. The mean stacking of the MoS_2 fringes on this catalyst was about 7 layers. HR-TEM images for NiMoS/TiMg 15 are presented in Fig. 8. A mean of 5 stacked layers of metal sulfides was calculated. Figures 9 and 10 show some HR-TEM images of the NiW supported nanocatalysts. An interplanar distance of 6.2 and 6.4 Å and a mean stacking value of metal-sulphide

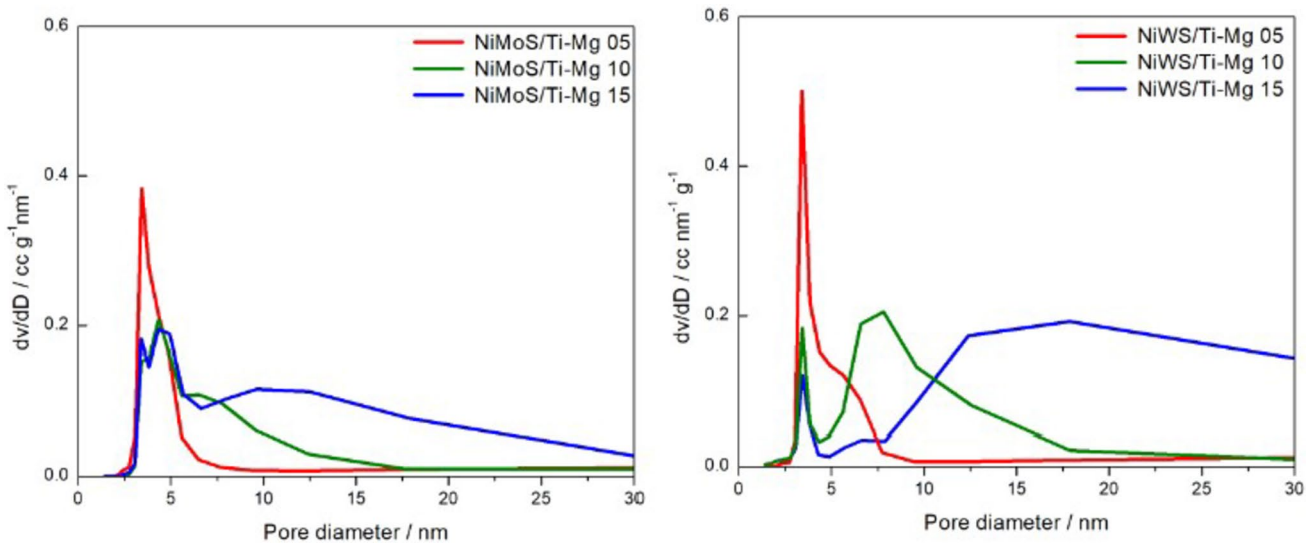

Fig. 6 Pore size distribution of the NiMoS/TiMg and NiWS/TiMg catalysts

Table 2 Specific surface areas, mean pore volume and diameter of the NiMoS/TiMg and NiWS/TiMg catalysts

Catalyst	Specific surface area (m^2/g)	Specific surface area loss (%)	Mean pore volume (cm^3/g)	Mean pore diameter (nm)
NiMoS/TiMg 05	45	48	0.07	3.4
NiMoS/TiMg 10	37	50	0.08	4.3
NiMoS/TiMg 15	44	30	0.11	3.4
NiWS/TiMg 05	38	56	0.12	3.4
NiWS/TiMg 10	52	30	0.08	3.4
NiWS/TiMg 15	50	20	0.09	3.4

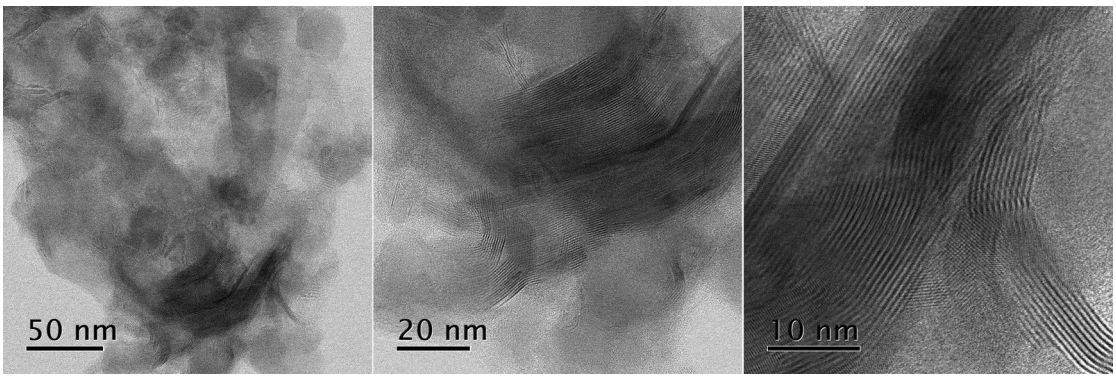

Fig. 7 HR-TEM images of the NiMoS/TiMg 5 catalyst

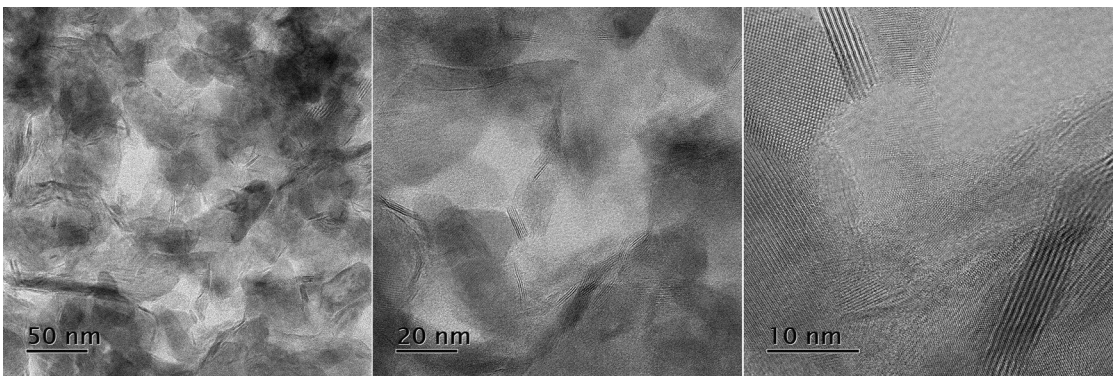

Fig. 8 HR-TEM images of the NiMoS/TiMg 15 catalyst

fringes of 3 and 5 layers were measured for NiWS/TiMg5 and NiWS/TiMg10 catalyst, respectively. The fringes observed on NiMoS/TiMg catalysts are straight, whereas those on NiWS/TiMg are curved. An increase of the Mg loading for the NiMoS/TiMg catalysts resulted in a decrease in the number of the stacked layers of the metal sulfide fringes whereas the opposite was noticed for the NiWS/TiMg catalysts. The length of the fringes was also determined and reported in Figs. 11 and 12 for molybdenum and tungsten catalysts, respectively. The fringes of about 12 nm that are observed for molybdenum catalyst containing 5 wt% of MgO are longer than those on the respective sample containing 15 wt% of MgO, though shorter fringes of about 6 nm are observed for tungsten catalyst containing 5 wt. % of MgO than those on the similar sample containing 10 wt% of MgO (Fig. 12). The tungsten nanocatalysts exhibited a mean value of 4 nm. The HR-TEM images for NiMoS/TiMg showed that an augmentation in the MgO contents from 5 to 15 wt% decreases the length of the MoS_2 fringes and the stacking, which is in agreement with the XRD results.

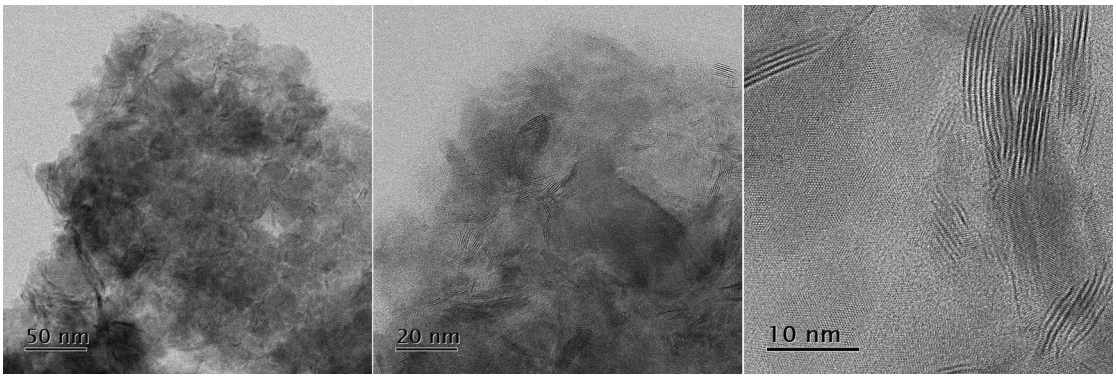

Fig. 9 HR-TEM images of the NiWS/TiMg 05 catalyst

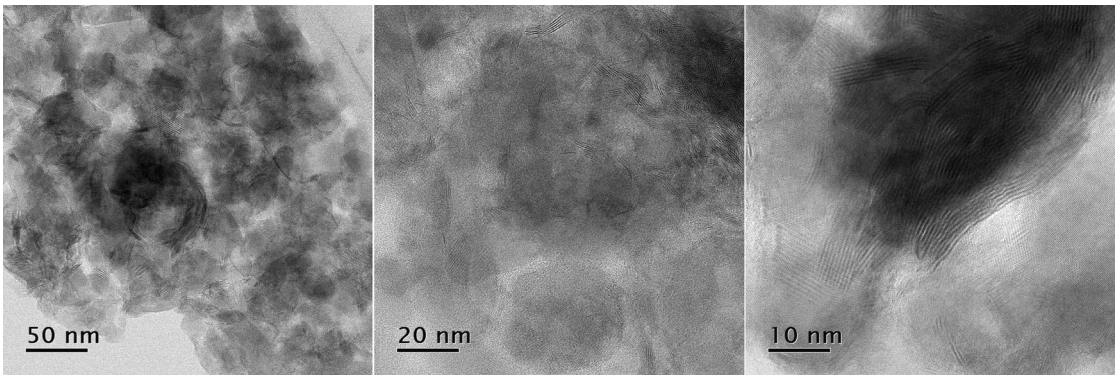

Fig. 10 HR-TEM images of the NiWS/TiMg 10 catalyst

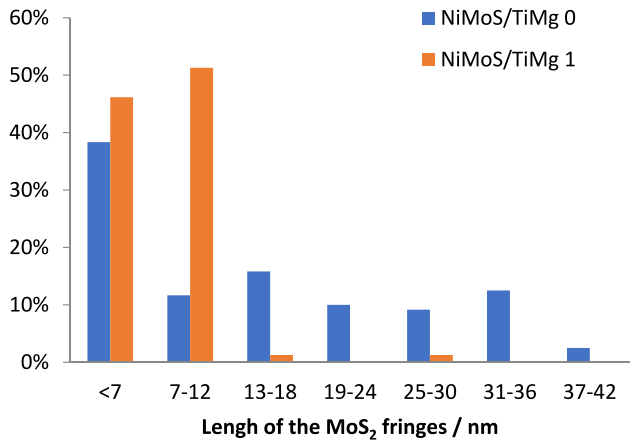

Fig. 11 Length distribution of the MoS_2 fringes for the NiMoS/TiMg 05 and NiMoS/TiMg 15 catalysts

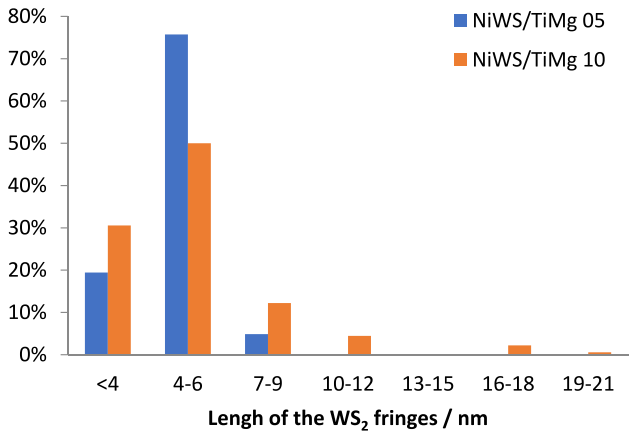

Fig. 12 Length distribution of the WS_2 fringes for the NiWS/TiMg 05 and NiWS/TiMg 10 catalysts

3.4 X-ray Photoelectron Spectroscopy

The sulfided NiMo and NiW supported catalysts were also analyzed by XPS. The scans exhibited the presence of core emission line regions for C 1*s*, O 1*s*, Ti 2*p*, Mg 2*p*, Ni 2*p* and depending upon composition, Mo 3*d* or W 4*f*. The determined surface composition is presented in Table 3. It is interesting to observe that the sulfur content decreases as the Mg augments for both Mo and W samples. As commented previously, the C 1*s* associated with the adventitious carbon was calibrated at 284.8 eV and the corresponding

Table 3 Elemental surface composition of NiMo/TiMg and NiWS/TiMg catalysts determined from the XPS data

Sample[a]	Element, atomic %						
	Ti	Mg	O	Ni	Mo	W	S
NiMo/TiMg-5	6.99	3.38	24.96	3.64	20.23	–	40.81
NiMo/TiMg-10	8.45	4.34	25.11	2.76	19.77	–	39.57
NiMo/TiMg-15	7.28	7.9	24.58	3.51	19.28	–	37.44
NiW/TiMg-5	9.98	2.36	32.5	2.66	–	12.79	39.72
NiW/TiMg-10	11.81	4.15	34.75	2.86	–	13.62	32.8
NiW/TiMg-15	13.17	8.55	40.86	2.65	–	9.45	25.32

[a]Samples were ex-situ sulfided at 400 °C with a H_2S/H_2 mixture of 15% v/v hydrogen balance

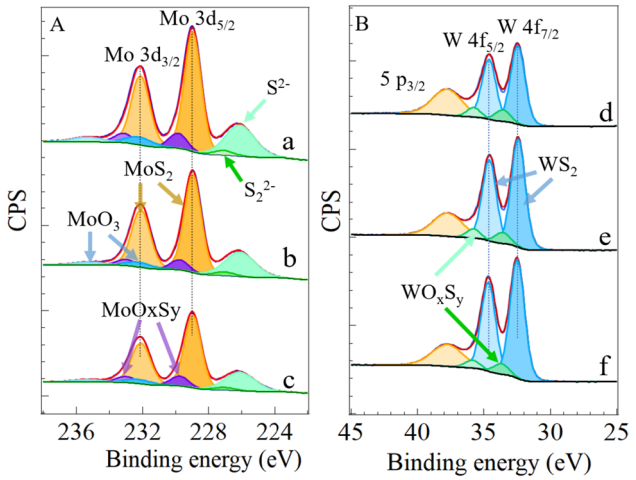

Fig. 13 Deconvolution of the Mo 3*d* and W 4*f* XPS spectra for NiMoS/TiMg-5, NiMoS/TiMg-10, NiMoS/TiMg-15 (**a**, **b**, **c**, respectively) and NiWS/TiMg-5, NiWS/TiMg-10 and NiWS/TiMg-15 (**f**, **e**, **d**, respectively)

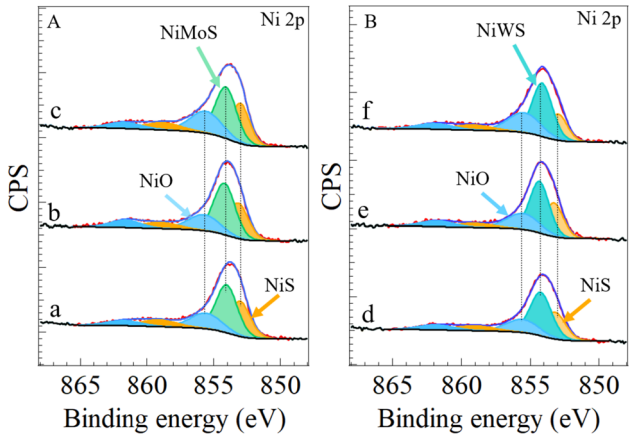

Fig. 14 Deconvolution of the Ni $2p_{3/2}$ XPS spectra for NiMoS/TiMg-5, NiMoS/TiMg-10, NiMoS/TiMg-15 (**a**, **b**, **c**, respectively) and NiWS/TiMg-5, NiWS/TiMg-10 and NiWS/TiMg-15 (**f**, **e**, **d**, respectively)

spectra are provided in the supplementary information as Fig. S1-a. Similarly, for O 1*s* core emission line region which shows a signal centered at 530.5 eV, the spectra are presented in Fig. S1-b. Figure 13 presents the XPS spectra and the fitting for the NiMoS and NiWS supported catalysts. Figure 13A shows the Gaussian-Lorentzian curve fitting of the Mo 3*d* core emission line region for the NiMoS supported samples. The assumption of the presence of MoO_3, MoO_xS_y, and MoS_2 species could well fit the XPS spectrum [19]. The characteristic doublet related to the Mo 3*d* region Fig. 13, comprises two peaks of Mo $3d_{5/2}$ at 229.1 eV and Mo $3d_{3/2}$ at 235.3 eV related to Mo^{4+} and Mo^{6+} respectively, whereas the peak at about 232.2 eV arises from the contribution of Mo^{4+}/Mo^{6+} oxysulfides [20]. The presence of S^{2-} and S_2^{2-} species related to S 2*s* electrons were also considered in this region. The abundance of Mo^{4+}species in all the NiMoS/TiMg samples is predominant. Accordingly to the determined areas of the peaks after deconvolution, the NiMoS/TiMg-5 sample contains 81.2, 11.5 and 7.3% of Mo^{4+}, Mo^{4+}/Mo^{6+} and Mo^{6+} species, respectively. The XPS region related to W 4*f* is presented in Fig. 13B for the NiWS/TiMg catalysts. Consistently with the literature, the W $4f_{5/2}$ binding energies for W^{6+}, W^{5+} and W^{4+} species are located at 38.0, 37.8 and 34.4 eV, respectively, and their W $4f_{7/2}$ at 35.6, 33.5, and 32.2 eV, respectively [21, 22]. However, two peaks at about 32.9 and 34.7 eV assigned to W $4f_{7/2}$ and W $4f_{5/2}$ and another at 37.7 eV assigned to the W $5p_{3/2}$ level, were observed in our spectra. After deconvolution, two small peaks at the binding energies of 33.7 eV and 35.9 eV resulted which were assigned to the WO_xS_y (W^{5+} species). The W^{6+} species such as WO_3, were absent in our samples. Figure 14 presents the XPS spectra and the deconvolution of the Ni 2*p* region for the NiMo/TiMg (Fig. 14A) and NiW/TiMg (Fig. 14B) catalysts. Table 4 shows surface phase composition resulted from the XPS deconvolution. The S 2*p* region of the XPS spectra presents only one peak at 162 eV (Fig. S2). The intensity of the signal at about 162 eV decreases as the Mg content augments, suggesting a decrease in sulfidation of the metal oxides. The Ti 2*p* and Mg 2*p* regions of the XPS spectra are also included in the supplementary information (Figs. S3 and S4). A peak at about 459.2 eV assigned to Ti $2p_{3/2}$ shows only slightly variations

Table 4 Mo, W and Ni surface species determined from the deconvolution of the respective regions of the XPS spectra

Sample	Mo 2*p*			W 4*f*			Ni $2p_{3/2}$		
	MoO_3	MoO_xS_y	MoS_2	WO_3	WO_xS_y	WS_2	NiO	NiMo(W)S	NiS
NiMo/TiMg-5	7.3	11.5	81.2	–	–	–	22.1	46.0	31.9
NiMo/TiMg-10	7.3	9.0	83.7	–	–	–	21.4	47.7	30.9
NiMo/TiMg-15	8.4	8.3	83.3	–	–	–	27.5	43.8	28.7
NiW/TiMg-5	–	–	–	–	8.5	91.5	23.9	47.6	28.5
NiW/TiMg-10	–	–	–	–	9.9	90.1	22.0	49.4	28.7
NiW/TiMg-15	–	–	–	–	13.5	86.5	29.1	49.7	21.2

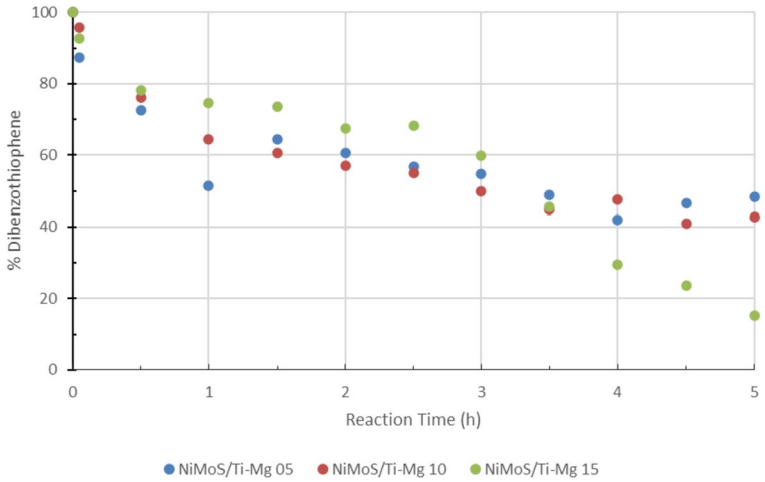

Fig. 15 DBT conversion as function of time for the NiMoS/TiMg catalysts

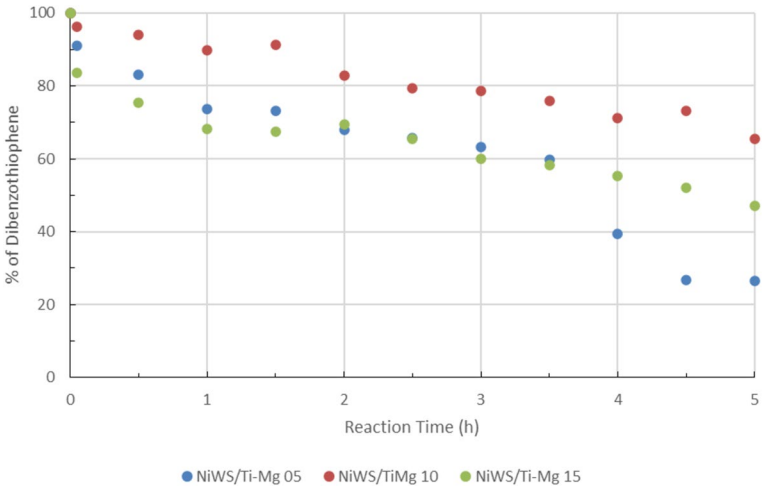

Fig. 16 DBT conversion as function of time for the NiWS/TiMg catalysts

in intensity as the sample composition varies. In addition, the intensity of the signal at about 50.3 eV attributed to Mg 2*p* increases as the content of this element augments.

3.5 Catalytic Activity and Selectivity

According to the behavior of the catalytic activity as a function of time, a pseudo-first order rate expression was proposed to represent the experimental data which exhibit good fitting. Figures 15 and 16 show the transformation of DBT as a function of time for the NiMoS/TiMg and NiWS/TiMg nanocatalysts, respectively, whereas Figs. 17 and 18 show the selectivity of both series of catalysts as function of the DBT conversion. Comparing tungsten and titanium samples, the selectivity increases as the MgO augments for the latter series, whereas for the former remain practically unchanged. Table 5 presents the conversion of DBT in percentages, the calculated reaction rate coefficients,

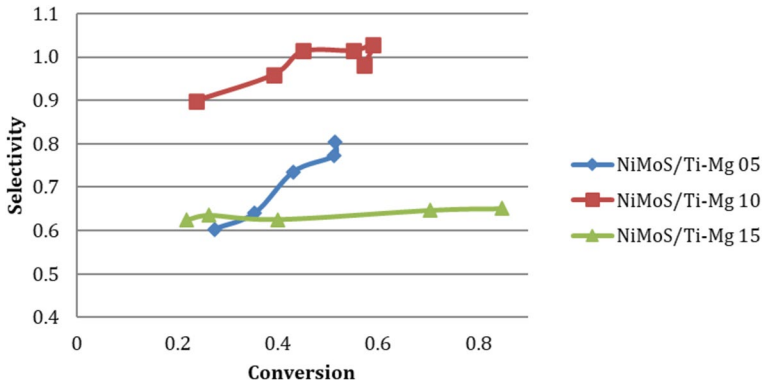

Fig. 17 Selectivity as function of DBT conversion for the NiMoS/TiMg catalysts during the HDS of DBT

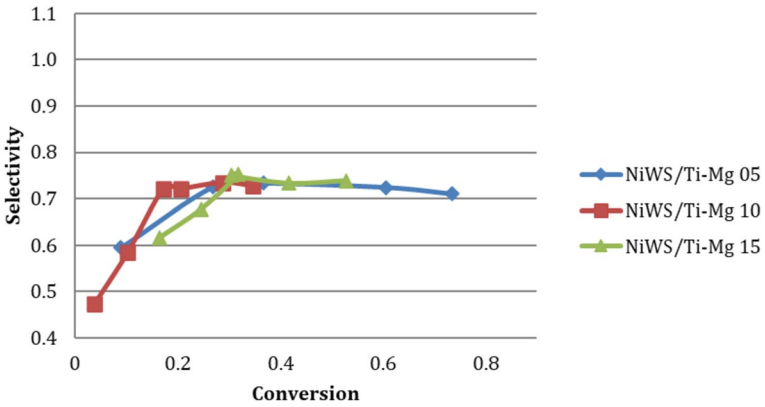

Fig. 18 Selectivity as function of DBT conversion for the NiWS/TiMg catalysts during the HDS of DBT

Table 5 DBT conversion (%), reaction rate constants (k) and selectivities (HYD/DDS) for the NiMoS/TiMg, NiWS/TiMg, $NiMoS/TiO_2$ and $NiWS/TiO_2$ catalysts

Catalyst	DBT conversion (%)	k x 10^{-7} $(s)^{-1}$	HYD/DDS
$NiMoS/TiO_2$	12.8	2.7	0.50
NiMoS/TiMg 05	51.6	8.4	0.80
NiMoS/TiMg 10	57.2	10.3	0.98
NiMoS/TiMg 15	74.1	15.1	0.68
$NiWS/TiO_2$	34.8	5.6	0.55
NiWS/TiMg 05	73.5	12.9	0.71
NiWS/TiMg 10	34.6	6.2	0.72
NiWS/TiMg 15	52.8	7.6	0.73

evaluated assuming a pseudo-first order rate equation, and the selectivity (HYD/DSD). The main reaction products were CHB and BF. However, small quantities of THDBT were detected. As a reference, the catalytic activities of $NiMo/TiO_2$ and $NiWS/TiO_2$ are also included in this table. As it can be observed, both catalysts presented very low DBT conversions compared to those with Mg, indicating a positive effect of this element in both series of catalysts. For NiMoS/TiMg the improvement in the catalytic activity went form 51% DBT conversion to 84% when the MgO increases from 5 to 15 wt%. The best catalyst of this series was the NiMoS/TiMg 15 sample with a 74.1% DBT conversion at 5 h. The XRD and HR-TEM results indicated that the positive effect of Mg in the NiMoS/TiMg samples is likely related to a better dispersion of the active sulfide species. The intensity of the X-ray diffraction assigned to MoS_2 and the length and stacking of the MoS_2 fringes decrease when Mg augments. However, the enhancement in the HDS activity, which is also observed in the NiWS samples by using Mg, seems to be related to a different phenomenon. Unlikely the behaviour of the molybdenum catalysts, the tendency in the catalytic activity as function of the Mg loadings was different for the tungsten catalysts. Among this series of samples, the highest DBT conversion of 73.5% at 5 h was observed for the NiWS/TiMg 05 with a reaction rate coefficient of 12.9×10^{-7} s^{-1}. Contrarily to the best molybdenum catalyst, NiWS/TiMg 05 presents the minimum Mg loading. The HDS activity of this sample might be related to the highest sulfur contents on this catalyst determined by XPS. Nevertheless, more characterization is clearly required to elucidate this. Table 5 also indicates that independently of the Mg contents, both series of catalysts are more selective for the DDS than for the HYD pathway, as previously reported for NiMo/TiMg catalysts of different Ti/Mg ratio [23]. In addition, this effect is slightly more pronounced for the tungsten than for titanium samples.

4 Conclusions

NiMoS/TiMg and NiWS/TiMg nanocatalysts with various Mg loading were synthesized and tested in the HDS of DBT. Similar catalysts supported on pure TiO_2 were also tested and used as references. Both NiMo and NiW samples supported on pure titania showed lower HDS activities than those supported on TiMg mixed oxides, indicating a positive effect of Mg. Furthermore, the NiMoS/TiMg catalysts show higher HDS activities than those observed for the NiWS/TiMg samples. Among the catalysts reported herein, NiMoS/TiMg-15 and NiWS/TiMg-5 showed the highest DBT conversions of 74.1% and 73.5%, respectively, after 5 h of reaction at 350 °C and 3.1 bars. The increasing Mg presence induced considerable changes on the obtention of active phases, for example in the formation of the MoS_2 and WS_2. In the first case the MoS_2 represented almost 82% meanwhile the oxysulfur phase and MoO_3 phases represented the remaining 18%. In the case of W the sulfidation was almost complete since no WO_3 was observed and the quantification of the oxysulfide phase represented no more of 13%. This indicated that the W interact less strongly with the surface of support than Mo. This was also confirmed by the HRTEM analysis in which the Mo presented larger MoS_2 slabs than the WS_2. The results presented in this work indicated that these support samples are suitable to continue with the scaling experiments for a possible industrial application.

Supplementary Information The online version contains supplementary material available at https://doi.org/10.1007/s11244-024-01916-w.

Acknowledgements JNDL wants to thank Drs. David Dominguez and J.A. Díaz for their expert technical assistance, and Projects DGAPA-PAPIIT-IN-104122 and IA-100322. Dr. R. Huirache-Acuña wants to thank CIC-UMSNH 2024, ICTI PICIR-047 and ECOS NORD 2022 Projects for their financial support.

References

1. Dembaremba TO, Majodina S, Walmsley RS, Ogunlaja AS, Tshentu ZR (2022) Perspectives on strategies for improving ultra-deep desulfurization of liquid fuels through hydrotreatment: catalyst improvement and feedstock pre-treatment. Front Chem 10:807225
2. Hansmeier AR, Meindersma GW, de Haan AB (2011) Desulfurization and denitrogenation of gasoline and diesel fuels by means of ionic liquids. Green Chem 13:1907–1913
3. Eni (2021) Eni World oil, gas and renewables review. Annual Statistical Report
4. Castillo-Villalón P, Ramírez J, Cuevas R, Vázquez P, Castañeda R (2016) Influence of the support on the catalytic performance of Mo, CoMo, and NiMo catalysts supported on Al_2O_3 and TiO_2 during the HDS of thiophene, dibenzothiophene, or 4,6-dimethyldibenzothiophene. Catal Today 259:140–149
5. Absi-Halabi M, Stanislaus A, Al-Dolama K (1998) Performance comparison of alumina-supported Ni–Mo, Ni–W and Ni–Mo–W catalysts in hydrotreating vacuum residue. Fuel 77:787–790
6. Wang H, Prins R (2009) Hydrodesulfurization of dibenzothiophene, 4,6-dimethyldibenzothiophene, and their hydrogenated intermediates over Ni–MoS_2/γ-Al_2O_3. J Catal 264:31–43
7. Huirache-Acuña R, Albiter MA, Ornelas C, Paraguay-Delgado F, Martínez-Sánchez R, Alonso-Nuñez G (2006) Ni(Co)–Mo–W sulphide unsupported HDS catalysts by ex situ decomposition of alkylthiomolybdotungstates. Appl Catal A 308:134–142
8. Okamoto Y, Breysse M, Murali Dhar G, Song C (2003) Effect of support in hydrotreating catalysis for ultra clean fuels. Catal Today 86:1–3
9. Babich IV, Moulijn JA (2003) Science and technology of novel processes for deep desulfurization of oil refinery streams: a review. Fuel 82:607–631
10. Olguin E, Vrinat M, Cedeno L, Ramirez J, Borque M, López-Agudo A (1997) The use of TiO_2–Al_2O_3 binary oxides as supports for Mo-based catalysts in hydrodesulfurization of thiophene and dibenzothiophene. Appl Catal A 165:1–13
11. Cervantes-Gaxiola ME, Arroyo-Albiter M, Maya-Yescas R, Rico-Cerda JL, Guevara-Lara A, Espino-Valencia J (2012) Synthesis, characterization and catalytic activity during hydrodesulphurization of dibenzothiophene of NiMoW catalysts supported on AlTi mixed oxides modified with MgO. Fuel 100:57–65
12. Trejo F, Rana MS, Ancheyta J (2008) CoMo/MgO–Al_2O_3 supported catalysts: an alternative approach to prepare HDS catalysts. Catal Today 130:327–336
13. Klimova T, Casados D (1998) New selective Mo and NiMo HDS catalysts supported on Al_2O_3–MgO (x) mixed oxides. Catal Today 43:135–146
14. Guevara-Lara A, Cruz-Pérez AE, Contreras-Valdez Z, Mogica-Betancourt J, Alvarez-Hernández A, Vrinat M (2010) Effect of Ni promoter in the oxide precursors of MoS_2/MgO–Al_2O_3 catalysts tested in dibenzothiophene hydrodesulphurization. Catal Today 149:288–294
15. Mogica-Betancourt JC, López-Benítez A, Montiel-López JR, Massin L, Aouine M, Vrinat M, Berhault G, Guevara-Lara A (2014) Interaction effects of nickel polyoxotungstate with the Al_2O_3–MgO support for application in dibenzothiophene hydrodesulfurization. J Catal 313:9–23
16. Cruz Pérez AE, Torrez Jiménez Y, Velasco Alejo JJ, Zepeda TA, Frías Márquez DM, Rivera Ruedas MG, Fuentes S, Díaz de León JN (2016) NiW/MgO–TiO_2 catalysts for dibenzothiophene hydrodesulfurization: effect of preparation method. Catal Today 271:28–34
17. Semeykina VS, Parkhomchuk EV, Polukhin AV, Parunin PD, Lysikov AI, Ayupov AB, Cherepanova SV, Kaichev VV, Glazneva TS (2016) CoMoNi catalyst texture and surface properties in heavy oil processing. Part II: macroporous sepiolite-like mineral. Ind Eng Chem Res 55:9129–9139
18. Cervantes-Gaxiola ME, Arroyo-Albiter M, Pérez-Larios A, Balbuena PB, Espino-Valencia J (2013) Experimental and theoretical study of NiMoW, NiMo, and NiW sulfide catalysts supported on an AlTiMg mixed oxide during the hydrodesulfurization of dibenzothiophene. Fuel 113:733–743
19. Laurenti D, Phung-Ngoc B, Roukoss C, Devers E, Marchand K, Massin L, Lemaitre L, Legens C, Quoineaud A-A, Vrinat M (2013) Intrinsic potential of alumina-supported CoMo catalysts in HDS: comparison between Γc, ΓT, and δ-alumina. J Catal 297:165–175
20. Zhai P, Zhang Y, Wu Y, Gao J, Zhang B, Cao S, Zhang Y, Li Z, Sun L, Hou J (2020) Engineering active sites on hierarchical transition bimetal oxides/sulfides heterostructure array enabling robust overall water splitting. Nat Commun 11:5462

21. Reinhoudt HR, Crezee E, van Langeveld AD, Kooyman PJ, van Veen JAR, Moulijn JA (2000) Characterization of the active phase in NiW/γ-Al_2O_3 catalysts in various stages of sulfidation with FTIR(NO) and XPS. J Catal 196:315–329
22. Rodríguez-Castellón E, Jiménez-López A, Eliche-Quesada D (2008) Nickel and cobalt promoted tungsten and molybdenum sulfide mesoporous catalysts for hydrodesulfurization. Fuel 87:1195–1206
23. López-Benítez A, Berhault G, Silva-Rodrigo R, Rodríguez-Ávila JA, Vrinat M, Guevara-Lara A (2019) Evaluation of the interest of NiMo catalysts supported on MgO–TiO_2 for hydrodesulfurization applications. Catal Lett 149:2656–2670

Authors and Affiliations

P. Peña-Obeso[1] · M. E. Cervantes-Gaxiola[2] · J. L. Rico[1] · J. N. Díaz de León[3] · S. Guevara-Martinez[1] · J. A. Lumbreras-Pacheco[1] · R. Huirache-Acuña[1]

✉ R. Huirache-Acuña
rafael_huirache@yahoo.it

[1] Facultad de Ingeniería Química, Universidad Michoacana de San Nicolás de Hidalgo, Ciudad Universitaria, C.P. 58060 Morelia, Mexico

[2] Facultad de Ciencias Químico Biológicas, Ingeniería Química. Circuito, Universidad Autónoma de Sinaloa, Cd Universitaria, C.P. 80040 Culiacán Rosales, Mexico

[3] Universidad Nacional Autónoma de México (UNAM)-Centro de Nanociencias y Nanotecnología (CNyN), Km. 107 Carretera Tijuana-Ensenada Col. Pedregal Playitas, C.P. 22860 Ensenada, Baja California, Mexico